Cross-Modal Mapping: Mitigating the Modality Gap for Few-Shot Image Classification

Xi Yang[1] **Pai Peng**[1] **Wulin Xie**[1] **Xiaohuan Lu**[1] **Jie Wen**[2*]

[1]Guizhou University, Guiyang, China
[2] Harbin Institute of Technology, Shenzhen, China

jiewen_pr@126.com

Abstract

Few-shot image classification remains a critical challenge in the field of computer vision, particularly in data-scarce environments. Existing methods typically rely on pre-trained visual-language models, such as CLIP. However, due to the modality gap, which is the inconsistent distribution of image and text features in the joint embedding space, directly using these features as class prototypes often leads to suboptimal performance. To address this issue, we propose a novel Cross-Modal Mapping (CMM) method. This method globally aligns image features with the text feature space through linear transformation and optimizes their local spatial relationships using triplet loss, thereby significantly enhancing cross-modal consistency. Experimental results show that compared to other methods, CMM simplifies the training process and demonstrates higher efficiency. Furthermore, CMM improves the average Top-1 accuracy by 1.06% on 11 benchmark datasets compared to methods that partially fine-tune the backbone, and it performs excellently on 4 distribution shift datasets. Notably, CMM effectively mitigates the modality gap in pre-trained models, enabling text features to serve as effective class prototypes for image features, thus providing an efficient and highly generalizable solution for few-shot learning.

1 Introduction

Few-shot image classification is a pivotal challenge in computer vision, aiming to classify new image categories with only a handful of labeled samples. This task is vital in data-scarce domains like medical image analysis (Milletari et al., 2016), wildlife recognition (Zheng, 2022), and rare object detection (Wang et al., 2020), where large labeled datasets are costly or infeasible to obtain. Consequently, designing models with robust generalization under limited data is a critical research focus.

Recent advances have utilized pre-trained visual-language models (VLMs) (Chen et al., 2021; Yuan et al.), such as CLIP (Radford et al., 2021), which aligns image and text modalities in a joint embedding space through contrastive learning on a large number of image-text pairs. This alignment promises effective few-shot classification by leveraging pre-trained representations. However, a modality gap persists, defined as the inconsistent distribution of image and text features in this space, as illustrated in Fig. 1 (left). This gap arises from the different ways CLIP processes visual and textual inputs and the inherent limitations of contrastive loss, leading to separate clustering of image and text features. This distributional inconsistency is particularly pronounced in fine-grained tasks, such as bird species classification, where subtle visual distinctions (e.g., beak shape) may not align with textual descriptions. When text features serve as class prototypes in few-shot settings, this misalignment amplifies such errors.

Existing methods often fail to fully consider the issue of modality gap in their design, and their efficiency performance varies significantly. For example, CoOp (Gu et al., 2021) optimizes context prompts for specific categories by learning additional text embeddings to enhance text adaptability, but this process significantly increases training time and does not involve optimizing image features.

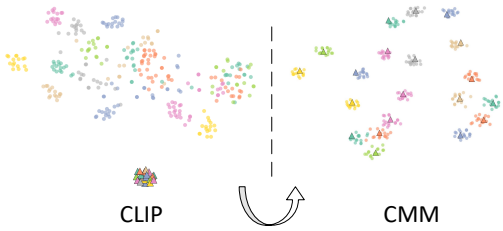

Figure 1: T-SNE Maaten & Hinton (2008) Visualization: Triangles represent textual feature embeddings for each category, dots indicate image feature embeddings, and different colors distinguish various categories.

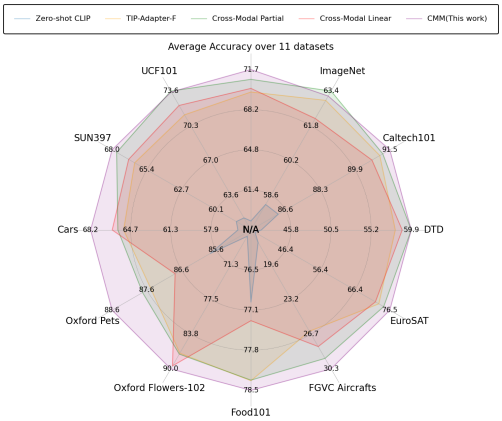

Figure 2: CMM demonstrates competitive performance across 11 datasets, with values reflecting the average top-1 accuracy under 1, 2, 4, 8, and 16-shot conditions compared to other methods.

In contrast, cache-based methods (such as Tip-Adapter (Zhang et al., 2021)) adapt to CLIP by repeatedly building key-value caches using data augmentation from the training set. However, their computational process within the visual modality is relatively slow, leading to low efficiency, and they also do not optimize text features. Therefore, both methods fail to effectively mitigate the gap between image and text modalities, thereby limiting semantic richness and highlighting their respective limitations in efficiency.

To overcome the aforementioned limitations, we propose Cross-Modal Mapping (CMM), a method designed to mitigate the modality gap while achieving high generalization and computational efficiency. CMM employs linear transformations to achieve global alignment of image and text features and utilizes triplet loss to locally refine their spatial relationships (as shown in Fig. 1, right). This dual strategy effectively reduces the modality gap, enabling text features to serve as precise class prototypes. Furthermore, the reduction in the modality gap significantly narrows the hyperparameter space required for integrating the original CLIP outputs (Zhang et al., 2021), and only necessitates optimizing the linear transformation matrix and text features, thereby substantially reducing computational overhead. This efficient and adaptable design makes CMM particularly suitable for data-scarce scenarios.

As shown in Fig. 3, CMM demonstrates competitive performance in few-shot tasks. Compared to the method of partially fine-tuning the backbone (Lin et al., 2023), CMM improves the average top-1 accuracy by 1.06% across 11 datasets (Fig. 2). These results demonstrate the effectiveness of CMM.

Our contributions are summarized as follows:

- We systematically investigate the impact of the modality gap on class prototypes in pre-trained vision-language models (VLMs), revealing its detrimental effects in few-shot image classification.

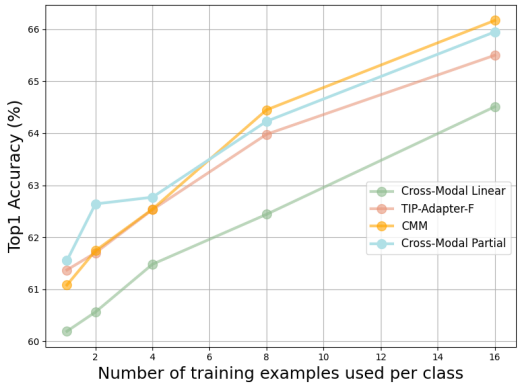

Figure 3: Performance comparison of CMM, TIP (Zhang et al., 2021), and Cross-Modal Linear/Partial (Lin et al., 2023) on ImageNet. CMM outperforms partial fine-tuning approaches.

- We propose the Cross-Modal Mapping (CMM) method, which significantly reduces the modality gap through the optimization of a linear transformation and triplet loss, achieving exceptional few-shot classification performance across multiple datasets.
- CMM offers an efficient and highly generalizable solution that avoids overfitting and high computational costs, advancing the application of VLMs in data-scarce scenarios.

2 Related Work

Few-Shot Classification aims to enable models to effectively classify using only a limited number of labeled samples. Traditionally, this field has primarily relied on methods such as metric learning (Ermolov et al., 2022; Cai et al., 2023) and meta-learning (Yu et al., 2020; Yang et al., 2020). Metric learning approaches, such as Matching Networks (Vinyals et al., 2016), Prototypical Networks (Snell et al., 2017), and Relation Networks (Palm et al., 2018), focus on learning an embedding space where samples from the same class are closer in position, while samples from different classes are farther apart. For example, Prototypical Networks compute a prototype vector for each class and classify query samples based on their distance (typically using cosine similarity) to these prototypes. Meta-learning methods, such as MAML (Finn et al., 2017) and Meta-SGD (Li et al., 2017), optimize initial parameters across meta-tasks to enable rapid adaptation to new tasks. Although these traditional methods are effective to some extent, they often involve complex training procedures and high computational costs. In recent years, the rise of pre-trained vision-language models has shifted this paradigm. By leveraging contrastive learning for large-scale pre-training, these models reduce the reliance on large amounts of labeled data, providing an efficient alternative for few-shot classification.

Pre-trained Vision-Language Models (e.g., CLIP (Radford et al., 2021)) have garnered significant attention for their ability to align visual and textual representations through training on large-scale image-text datasets. These models (Chen et al., 2021; Yuan et al.), developed using contrastive learning, excel in tasks such as zero-shot and few-shot classification by employing textual descriptions as class prototypes. In the realm of few-shot classification, their application is transformative, enabling models to adapt to new categories with minimal examples. Existing methods enhance their performance through techniques like prompt tuning (Zhu et al., 2023), where, for instance, CoOp (Gu et al., 2021) optimizes learnable prompts to fine-tune the model. Additionally, adapter methods (Sung et al., 2022; Zhang et al., 2021) insert and adjust lightweight modules within the model architecture to improve adaptability. However, despite their notable success, these models still suffer from an inherent modality gap, which hampers classification accuracy, particularly in few-shot scenarios. This limitation has prompted researchers to focus on addressing the modality gap and streamlining the training process to achieve rapid adaptation to new tasks.

The modality gap in pre-trained vision-language models refers to the imperfect alignment between visual and textual embeddings, which hinders effective cross-modal interaction. According to (Liang et al., 2022), its root cause lies in the model initialization and contrastive learning during pre-training.

Although CLIP establishes a joint embedding space to enable few-shot learning, the persistent cross-modal distance limits its performance. Researchers have proposed various methods to address this challenge. For instance, SgVA-CLIP (Peng et al., 2022) attempts to enhance feature alignment by using contrastive loss to mitigate the modality gap. However, the contrastive loss itself has limitations and will continue to lead to a modality gap. Similarly, (Lin et al., 2023) enables the model to better align representations from different modalities by using class names as additional single-sample training data. However, its effectiveness decreases if the representation spaces of different modalities are poorly aligned. Our proposed Cross-Modal Mapping (CMM) provides a direct and effective solution. By leveraging linear transformation and triplet loss, CMM achieves global alignment and local optimization, outperforming existing methods.

3 Method

In this section, we first outline our motivation for tackling the modality gap in VLMs, followed by an in-depth explanation of the Cross-Modal Mapping (CMM) method, covering its architecture and implementation details.

3.1 Motivation

In recent years, methods utilizing pre-trained vision-language models (such as CLIP) for few-shot image classification have achieved significant progress in data-scarce scenarios. These methods accomplish category recognition by computing the similarity between image features and text features. However, existing approaches often neglect the modality gap between image features and text features, which manifests as inconsistencies in their distributions within the joint embedding space. A detailed analysis of this issue is provided in Section 4.3.

We assume that image features v_i and text features t_k each follow Gaussian distributions, denoted as $v_i \sim \mathcal{N}(\mu_v, \Sigma_v)$ and $t_k \sim \mathcal{N}(\mu_t, \Sigma_t)$. The modality gap can be quantified using the Kullback-Leibler (KL) divergence between these two distributions:

$$D_{KL}(\mathcal{N}(\mu_v, \Sigma_v)||\mathcal{N}(\mu_t, \Sigma_t)), \tag{1}$$

where a smaller KL divergence indicates greater similarity between the distributions of text and image features. Nevertheless, in few-shot learning, the scarcity of data renders it impractical to directly estimate distribution parameters (e.g., VAE (Kingma & Welling, 2013)) and optimize the KL divergence. Such an approach results in unreliable distribution estimates, high computational complexity, and a misalignment between the optimization objective and the task requirements.

To address this challenge, we propose a novel Cross-Modal Mapping (CMM) method, which leverages supervised signals to indirectly achieve distribution alignment rather than directly optimizing the KL divergence. The method employs a linear transformation to provide global distribution alignment, while the triplet loss ensures local consistency within each category. By synergistically optimizing these two components, CMM enhances cross-modal consistency, enabling text features to serve as robust class prototypes and thereby improving the performance of few-shot image classification. This approach overcomes the limitations of existing methods, offering a simple, efficient, and generalizable solution.

3.2 Cross-Modal Mapping

As illustrated in Fig. 4, we propose a simple yet powerful Cross-Modal Mapping (CMM) method to mitigate the modality gap in pre-trained vision-language models, enabling textual features to act as dependable class prototypes.

To fully leverage textual information, we construct a text feature matrix for all categories using manually crafted templates from (Zhang et al., 2021). For each category c_k, we generate textual descriptions using these templates, which are then encoded into text features by a pre-trained text encoder. Formally, we define the text encoding operator $\mathcal{E}_{\text{text}} : \mathcal{T} \to \mathbb{R}^d$, where $\mathcal{T}$ represents the space of all possible text sequences, and $\mathbb{R}^d$ is the d-dimensional real vector space. Additionally, $\phi_m : C \to \mathcal{T}$ denotes the m-th template application function, mapping a category c_k to a specific text sequence. The text feature for category c_k under the m-th template is expressed as:

$$t_k^{(m)} = \mathcal{E}_{\text{text}} \circ \phi_m(c_k). \tag{2}$$

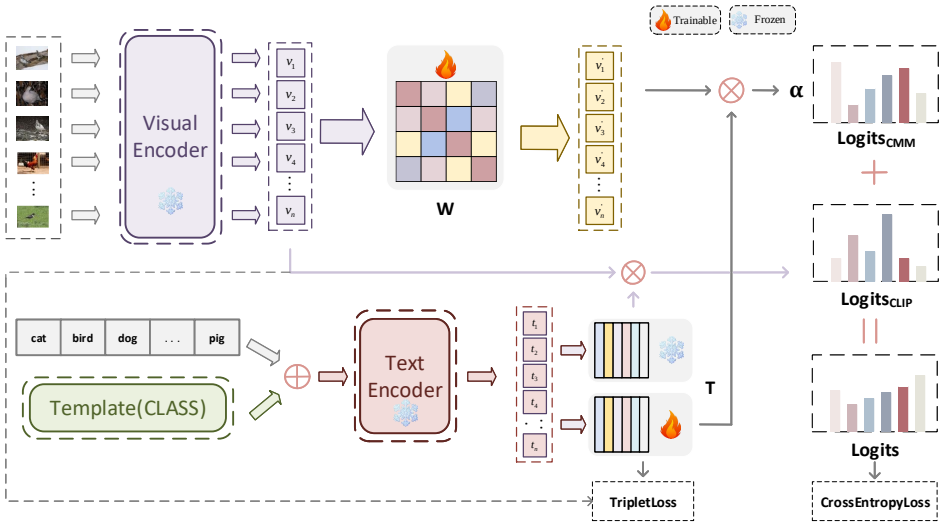

Figure 4: Cross-Modal Mapping (CMM) Architecture. Without the need to construct a visual cache, CMM optimizes only the linear transformation matrix W and the textual feature matrix T, simplifying the training process and effectively reducing the modality gap. This reduction in the modality gap narrows the search space for the fusion parameter α, thereby enhancing inference efficiency. $\text{Logits}_{\text{CLIP}}$ represents CLIP's inter-modal classification, while $\text{Logits}_{\text{CMM}}$ introduces a cross-modal inductive bias to further enhance classification capability.

Here, $t_k^{(m)} \in \mathbb{R}^d$ is the resulting d-dimensional feature vector for category c_k based on the m-th template. To form a comprehensive representation, we aggregate these text features into a matrix $\mathbf{T}_k = [t_k^{(1)}, t_k^{(2)}, \ldots, t_k^{(L)}]^T \in \mathbb{R}^{L \times d}$, where L is the total number of templates, and each row corresponds to a text feature from a specific template. We use a uniform weighting vector $\mathbf{u} = \frac{1}{L}\mathbf{1} \in \mathbb{R}^L$, where $\mathbf{1} = [1, 1, \ldots, 1]^T$ is a vector of ones, to compute the aggregated text feature:

$$t_k = \mathbf{u}^T \mathbf{T}_k. \tag{3}$$

This $t_k \in \mathbb{R}^d$ represents the averaged text feature across all L templates for category c_k. For scale consistency, we apply L2 normalization with the operator $\text{norm} : \mathbb{R}^d \to \mathbb{S}^{d-1}$, defined as $\text{norm}(\mathbf{v}) = \mathbf{v}/\|\mathbf{v}\|_2$, where $\mathbb{S}^{d-1}$ is the $(d-1)$-dimensional unit hypersphere. Thus, the normalized text feature $\hat{t}_k = \text{norm}(t_k) = t_k/\|t_k\|_2$ lies in $\mathbb{S}^{d-1}$. We then assemble these normalized features for all N categories into an initial text feature matrix $T^{init} \in \mathbb{R}^{d \times N}$ using the concatenation operator $\text{Concat} : (\mathbb{R}^d)^N \to \mathbb{R}^{d \times N}$:

$$T^{init} = \text{Concat}(\{\hat{t}_k\}_{k=1}^N). \tag{4}$$

Here, T^{init} serves as both an initial prototype matrix for all categories and an optimizable parameter enriched with semantic content.

For an input image x_i, we extract its features $v_i \in \mathbb{R}^d$ using CLIP's image encoder, denoted as $\mathcal{E}_{\text{img}} : \mathcal{X} \to \mathbb{R}^d$, where $\mathcal{X}$ is the space of all possible images:

$$v_i = \mathcal{E}_{\text{img}}(x_i). \tag{5}$$

These features are normalized using norm, yielding $\hat{v}_i = \text{norm}(v_i) = v_i/\|v_i\|_2 \in \mathbb{S}^{d-1}$, ensuring unit norm. We then project these normalized image features into the text feature space using a linear transformation matrix $W \in \mathbb{R}^{d \times d}$, initialized with the Kaiming method (He et al., 2015). The residual-augmented transformation operator $\mathcal{L}_W : \mathbb{R}^d \to \mathbb{R}^d$ is defined as $\mathcal{L}_W(\mathbf{v}) = \mathbf{v}(W + I_d)$, where $I_d \in \mathbb{R}^{d \times d}$ is the identity matrix. The mapped feature is:

$$v_i' = \mathcal{L}_W(\hat{v}_i) = \hat{v}_i(W + I_d). \tag{6}$$

Here, W is responsible for adjusting the distribution of image features to approximate that of the text feature space, while I_d preserves the foundational knowledge from the pre-trained model. Residual connections have been widely proven to improve gradient flow (He et al., 2016), preventing gradient

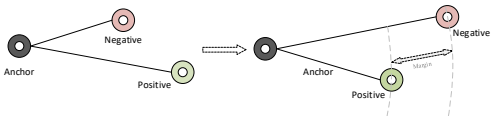

Figure 5: Triplet Loss: The anchor is the image feature, the positive is the corresponding textual feature, and the negative is the closest incorrect textual feature.

vanishing or exploding issues during training, and this stability is particularly crucial for effectively optimizing W. Furthermore, linear transformations are simpler and less prone to overfitting in data-scarce scenarios, a point that has been demonstrated in few-shot learning research Snell et al. (2017). In contrast, nonlinear transformations may distort certain geometric relationships, thereby reducing the alignment between image and text features. We provide a comparative analysis of nonlinear transformations in Appendix 7.1, further validating the advantages of linear transformations.

Subsequently, the mapped feature is normalized as $\hat{v}_i' = \text{norm}(v_i') = v_i'/\|v_i'\|_2 \in \mathbb{S}^{d-1}$. Similarity scores between $\hat{v}_i'$ and the fine-tuned text feature matrix $T^{ft} \in \mathbb{R}^{d\times N}$ are computed using the similarity functional $\mathcal{S} : \mathbb{R}^d \times \mathbb{R}^{d\times N} \to \mathbb{R}^N$, defined as:

$$s_i = \mathcal{S}(\hat{v}_i', T^{ft}) = \hat{v}_i' T^{ft}. \tag{7}$$

Here, $s_i \in \mathbb{R}^N$ represents the similarity scores across all N categories. The cross-modal classification logits are derived using the softmax operator $\sigma_\tau : \mathbb{R}^N \to \Delta^{N-1}$, where Δ^{N-1} is the $(N-1)$-dimensional probability simplex:

$$\text{Logits}_{\text{CMM}}(y = c_k|x_i) = \sigma_\tau(s_i)_k = \frac{\exp(s_{i,k}/\tau)}{\sum_{j=1}^N \exp(s_{i,j}/\tau)}. \tag{8}$$

In this expression, $\tau > 0$ is a temperature parameter controlling the smoothness of the probability distribution, and the subscript k extracts the k-th element corresponding to category c_k.

Despite mapping image features to the text domain achieving global alignment, residual local biases may persist, thereby affecting the alignment. To address this issue, we introduce the triplet loss to optimize the local alignment between image features and text features. Specifically, we use the cosine distance metric $d_{\cos} : \mathbb{S}^{d-1} \times \mathbb{S}^{d-1} \to [0, 2]$, which is defined as:

$$D_{i,k} = d_{\cos}(\hat{v}_i, \hat{t}_k) = 1 - \hat{v}_i^T \hat{t}_k. \tag{9}$$

This $D_{i,k}$ measures the distance between the normalized image feature $\hat{v}_i$ and the normalized text feature $\hat{t}_k$. The positive sample distance, where y_i is the true category of x_i, is:

$$D_{\text{pos}}^{(i)} = d_{\cos}(\hat{v}_i, \hat{t}_{y_i}), \tag{10}$$

and the hardest negative sample distance is:

$$D_{\text{neg}}^{(i)} = \min_{k\in\{1,\ldots,N\}\setminus\{y_i\}} d_{\cos}(\hat{v}_i, \hat{t}_k). \tag{11}$$

Using the hinge loss operator $[\cdot]_+ : \mathbb{R} \to \mathbb{R}_{\geq 0}$, where $[x]_+ = \max\{0, x\}$, the per-sample triplet loss is:

$$L_{\text{triplet}}^{(i)} = \left[D_{\text{pos}}^{(i)} - D_{\text{neg}}^{(i)} + \text{margin}\right]_+. \tag{12}$$

Here, margin > 0 is a hyperparameter enforcing a separation between positive and negative distances. The total triplet loss is averaged over a batch of size B:

$$L_{\text{triplet}} = \frac{1}{B}\sum_{i=1}^{B} L_{\text{triplet}}^{(i)}. \tag{13}$$

As shown in Figure 5, by enhancing the similarity of positive pairs, reducing the similarity of negative pairs, and introducing class constraints, the triplet loss can effectively reduce the local biases between image and text features.

3.3 Inductive Bias Incorporation

To leverage the zero-shot capabilities of pre-trained vision-language models (Radford et al., 2021), we incorporate $\text{Logits}_{\text{CMM}}(x)$ as a robust inductive bias (Tang et al.) alongside CLIP's $\text{Logits}_{\text{CLIP}}(x)$. We define a fusion operator $\mathcal{F}_\alpha : \mathbb{R}^N \times \mathbb{R}^N \to \mathbb{R}^N$ as $\mathcal{F}_\alpha(\mathbf{a}, \mathbf{b}) = \alpha\mathbf{a} + \mathbf{b}$, where $\mathbf{s}_{\text{CMM},i} = \mathcal{S}(\text{norm}(\mathcal{L}_W(\hat{v}_i)), T^{ft})$ represents the CMM similarity scores, and $\mathbf{s}_{\text{CLIP},i}$ denotes CLIP's raw inter-modal scores. The combined logits are:

$$\text{logits}_i = \mathcal{F}_\alpha(\mathbf{s}_{\text{CMM},i}, \mathbf{s}_{\text{CLIP},i}). \tag{14}$$

During training, we set $\alpha = 1.0$. For inference, we fine-tune α via a grid search over the range $[0.1, 1.0]$ with a step size of 0.1 on the validation set. This fusion retains CLIP's zero-shot advantages while enhancing the final classification capability. Due to the reduction in the modality gap, the search space for α is significantly narrowed. Compared to Zhang et al. (2021), this significantly reduces the inference overhead. We provide the optimal α found for each dataset in Appendix 7.2.

The final logits $\text{logits}_i \in \mathbb{R}^N$ are used to compute the cross-entropy loss with the log-softmax function $\text{logsoftmax} : \mathbb{R}^N \to \mathbb{R}^N$, defined as $\text{logsoftmax}(\mathbf{z})_k = z_k - \log(\sum_{j=1}^{N} \exp(z_j))$:

$$L_{CE} = -\frac{1}{B} \sum_{i=1}^{B} \text{logsoftmax}(\text{logits}_i)_{y_i}. \tag{15}$$

Here, y_i is the true label for sample x_i, and B is the batch size. The total CMM loss integrates both objectives:

$$L = L_{CE} + L_{\text{triplet}}. \tag{16}$$

In the training process, only the parameters W and T^{init} are optimized. The matrix W, by performing a linear transformation to adjust its distribution to approximate that of the text features, achieves global macroscopic alignment. Meanwhile, T^{ft} (the fine-tuned version of T^{init}) refines the class representations. Additionally, the triplet loss introduces category constraints, further reducing the local discrepancies between these distributions. We provide a computational complexity analysis in Appendix 7.4.

Algorithm 1 Pseudocode for Cross-Modal Mapping. Here, we can pre-extract intermediate features for training.

Training:
Initialize W, T^{init}
for each epoch and batch **do**
  $\hat{v}' = \text{norm}(\hat{v}(W + I_d))$
  $\mathbf{s}_{\text{CMM}} = \hat{v}' T^{ft}$
  $\mathbf{s}_{\text{CLIP}} = \text{Logits}_{\text{CLIP}}(x)$
  $\text{logits} = \alpha\mathbf{s}_{\text{CMM}} + \mathbf{s}_{\text{CLIP}}$
  Compute L_{CE}, L_{triplet}
  $L = L_{CE} + L_{\text{triplet}}$
  Update W, T^{ft}
end for
Inference:
Fine-tune α, classify with fused logits

4 Experiments

4.1 Experimental Settings

To fairly evaluate the performance of CMM in few-shot image classification tasks, we adopt the CoOp (Gu et al., 2021) protocol for assessment. In the settings of 1-shot, 2-shot, 4-shot, 8-shot, and 16-shot, we apply a complete flip ($p = 1.0$) to each sample as data augmentation. Additionally, we use the AdamW (Loshchilov, 2017) optimizer with a learning rate set at $1e-4$, weight decay of $1e-4$, and after 50 linear warm-up epochs, we employ a cosine annealing scheduler (Loshchilov & Hutter, 2016) with a minimum learning rate of $1e-5$. During the training phase, the batch size is

set at 8, with a total of 16,000 training iterations. The fusion coefficient α is fixed at 1.0, the margin in the triplet loss is set at 1.0, and the temperature parameter is consistent with that used in (Radford et al., 2021).

Datasets. We select 11 standard benchmark datasets covering a variety of image classification tasks, including Imagenet (Deng et al., 2009), Flowers102 (Nilsback & Zisserman, 2008), Caltech101 (Fei-Fei et al., 2004), FGVCAircraft (Maji et al., 2013), UCF101 (Soomro et al., 2012), EuroSAT (Helber et al., 2019), StanfordCars (Krause et al., 2013), DTD (Cimpoi et al., 2014), Food101 (Bossard et al., 2014), OxfordPets (Parkhi et al., 2012), and Sun397 (Xiao et al., 2010). These datasets encompass a wide range of task types such as large-scale image classification, fine-grained classification, texture classification, and satellite image classification, allowing for a comprehensive assessment of the CMM across different scenarios. To further evaluate the robustness of the CMM under distribution shifts, we have also chosen four distribution-shifted datasets: ImageNet-V2 (Recht et al., 2019) , ImageNet-Sketch (Wang et al., 2019) , ImageNet-A (Hendrycks et al., 2021b), and ImageNet-R (Hendrycks et al., 2021a). These datasets introduce new image styles, sketch versions, adversarial samples, and artistic style images, challenging the model's adaptability and generalization performance in the face of changes in data distribution.

4.2 Results

The average experimental results across various shots on the 11 standard benchmark datasets are shown in Table. 1. CMM outperforms comparative methods such as Adapter (Gao et al., 2024), Prompt Tuning (Zhou et al., 2022), cache-based adjustment (Zhang et al., 2021), and methods that further improve feature alignment through contrastive loss (Peng et al., 2022) in all settings. Additionally, its performance surpasses that of methods involving partial fine-tuning of the CLIP encoder (Lin et al., 2023) (with an overall average improvement of 1.06%). We also present the training duration in Table. 4, further illustrating the simplicity and efficiency of the CMM. Additionally, in Table. 2, we display the Top-1 accuracy of different architectural approaches in the 16-shot setting on ImageNet. These backbones have different embedding dimensions, indirectly reflecting the effectiveness between linear mapping and embedding dimensions. These results demonstrate that CMM contributes to mitigating the modality gap in pre-trained vision-language models.

Method	Number of shots					Train speed
	1	2	4	8	16	
Zero-Shot CLIP (58.8) (Radford et al., 2021)	-	-	-	-	-	-
Linear Probing	36.7	47.6	57.2	65.0	71.1	<1min
WiSE-FT (Wortsman et al., 2022)	59.1	61.8	65.3	68.4	71.6	<1min
CoOp (Gu et al., 2021)	59.6	62.3	66.8	69.9	73.4	14hr
ProGrad (Zhu et al., 2023)	62.6	64.9	68.5	71.4	74.0	17hr
Tip-Adapter (Zhang et al., 2021)	64.5	66.7	69.7	72.5	75.8	5min
Cross-Modal Linear Probing (Lin et al., 2023)	64.1	67.0	70.3	73.0	76.0	<1min
Cross-Modal Partial Finetuning (Lin et al., 2023)	64.7	67.2	70.5	73.6	77.1	<3min
SgVA-CLIP (Peng et al., 2022)	64.8	67.2	70.4	73.6	76.4	-
CMM	**65.5**	**68.6**	**71.8**	**74.9**	**77.6**	**<1min**

Table 1: Using RN50 (He et al., 2016), we compare the performance of different few-shot learning methods across 11 benchmarks under 1, 2, 4, 8, and 16-shot conditions, reporting the average accuracy for each shot condition along with the training speed.

In Table. 3, we further conduct an ODD assessment on ImageNet and report the performance of CMM under the RN50 (He et al., 2016). The experimental outcomes show that CMM exhibits competitive performance both within and across domains, proving its generalization capabilities in different fields and indicating that CMM has high robustness. In addition, we provide error case analysis in Appendix 7.5.

Models	RN50	RN101	V-B/16	V-B/32
Zero-shot CLIP (Radford et al., 2021)	60.33	62.53	68.73	63.80
CoOp (Gu et al., 2021)	62.95	66.60	71.92	66.85
CLIP-Adapter (Gao et al., 2024)	63.59	65.39	71.13	66.19
Tip-Adapter (Zhang et al., 2021)	62.03	64.78	70.75	65.61
Tip-Adapter-F (Zhang et al., 2021)	65.51	68.56	73.69	68.65
CMM	**66.17**	**68.93**	**74.23**	**69.17**

Table 2: Comparison of Top-1 accuracy across various methods on the ImageNet dataset using 16-shot learning with different architectures, where 'RN' represents ResNet and 'V-' represents ViT (Dosovitskiy, 2020).

	Source	**Target Datasets**			
	ImageNet	-V2	-A	-R	-Sketch
Linear-probe CLIP (Radford et al., 2021)	56.13	45.61	12.71	34.86	19.13
CoOp (Gu et al., 2021)	62.95	54.58	23.06	54.96	31.04
CoCoOp (Zhou et al., 2022)	62.81	55.72	23.32	57.74	34.48
Tip-Adapter (Zhang et al., 2021)	62.03	54.56	23.61	60.33	35.86
Tip-Adapter-F (Zhang et al., 2021)	65.51	56.79	20.93	58.48	34.62
Cross-Modal WiSE-FT(α=0.5) (Lin et al., 2023)	65.2	56.6	22.6	59.5	35.6
Cross-Modal Linear Probing (Lin et al., 2023)	64.5	55.3	20.0	56.4	33.1
CMM	**66.17**	**56.96**	**23.91**	**60.59**	**36.88**

Table 3: Comparison of Top-1 accuracy among various methods under distribution shifts using the RN50.

4.3 Analysis of inconsistent distributions.

The modality gap is specifically manifested as inconsistent distributions of image and text features in the shared embedding space. This gap originates from two main factors in pre-training:

Limitations of Contrastive Learning Objectives. Models like CLIP optimize a contrastive loss, encouraging:

$$\text{sim}(v_i, t_i) > \text{sim}(v_i, t_j) \quad \text{for} \quad i \neq j, \tag{17}$$

where v_i and t_i are image and text features of the i-th pair, and $\text{sim}(\cdot, \cdot)$ is a similarity function (e.g., cosine similarity). This is formalized as:

$$\mathcal{L}_{\text{contrastive}} = -\log \frac{\exp(\text{sim}(v_i, t_i)/\tau)}{\sum_{j=1}^{N} \exp(\text{sim}(v_i, t_j)/\tau)}, \tag{18}$$

where τ is a temperature parameter. While this objective aligns individual image-text pairs, it does not enforce global distributional alignment across modalities. As a result, systematic biases (such as different means or variances) still persist, leading to inconsistencies between the image feature distribution and the text feature distribution. For ease of analysis, we assume that $t_k \sim \mathcal{N}(\mu_t, \Sigma_t)$ and $v_i \sim \mathcal{N}(\mu_v, \Sigma_v)$. Then, Perfect alignment would require $\mu_v = \mu_t$ and $\Sigma_v = \Sigma_t$, but the contrastive loss only optimizes relative pairwise distances, not global statistical properties.

Modality-Specific Feature Extraction. Image encoders (e.g., ViT or ResNet) capture spatial hierarchies and visual patterns, generating features that cluster in the embedding space based on visual similarity (e.g., shared shapes or textures). In contrast, text encoders (e.g., Transformer) focus on semantic and syntactic relationships, generating features that cluster based on semantic proximity. Consequently, image features exhibit strong dimensional correlations tied to spatial layouts, while text features have more independent dimensions, each capturing distinct linguistic properties, leading to divergent and misaligned feature distributions in the joint embedding space.

Method	Iteration	Time	Accuracy	Gain
Zero-shot CLIP (Radford et al., 2021)	0	0	60.33	0
Image-Only Linear	12k	**15sec**	56.44	-3.89
CoOp (Gu et al., 2021)	100k	14h 40min	62.95	+2.62
ProGrad (Gu et al., 2021)	100k	17hr	63.45	+3.12
Tip-Adapter-F (Zhang et al., 2021)	10k	5min	65.51	+5.18
Cross-Modal Linear (Lin et al., 2023)	12k	**15sec**	64.51	+4.14
Cross-Modal Partial (Lin et al., 2023)	12k	2.5min	65.95	+5.57
CMM	16k	42sec	**66.17**	**+5.84**

Table 4: Performance comparison of various methods. Provides detailed information on the number of iterations, time taken, accuracy, and accuracy gain for each method. Notably, the CMM is tested with a batch size of 8, while other methods are tested with a batch size of 32. All tests are conducted on an NVIDIA 3090.

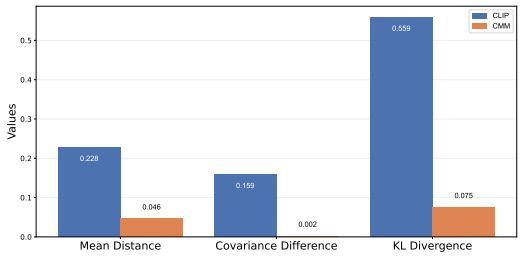

Figure 6: Comparison of distribution statistics of reduced dimensional features using KL divergence before and after applying CMM.

To quantify this gap, we calculate the KL divergence and Wasserstein-2 distance between image and text features on the ImageNet validation set. The KL divergence measures the difference between two probability distributions, reflecting the global inconsistency between the image and text feature distributions. The Wasserstein-2 distance further captures their geometric structural differences by measuring the optimal transport cost between the distributions. We use CLIP's image and text encoders to extract features and reduce their dimensionality to two using PCA. Then, we compute the Gaussian distribution parameters for the reduced image and text features using Maximum Likelihood Estimation (MLE). As shown in Figure 6, before applying CMM, there is a significant modality gap between the image and text feature distributions, characterized by significant differences in mean and covariance. After applying CMM, this gap is significantly reduced, and the distributions become closer.

However, the KL divergence calculated from the reduced features is only suitable for qualitative analysis and cannot fully capture the distribution differences in the original high-dimensional space. To address this issue, we further calculate the Wasserstein-2 distance on the original high-dimensional

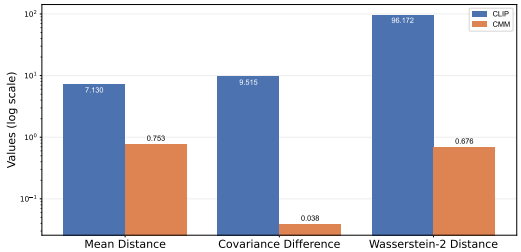

Figure 7: Comparison of distribution statistics of original features using the Wasserstein-2 distance before and after applying CMM.

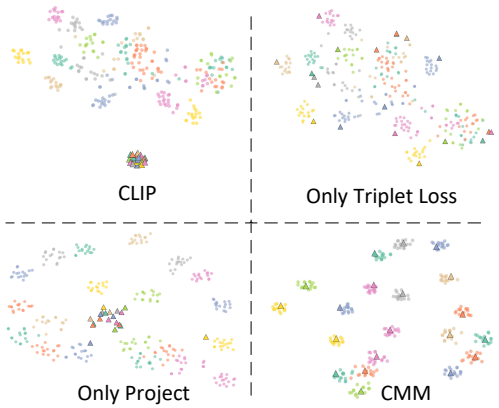

Figure 8: T-SNE Visualization for Ablation Study: Perplexity set to 40, iteration count set to 1000.

features to achieve a more precise quantitative assessment. As shown in Figure 7, after applying CMM, the Wasserstein-2 distance is significantly reduced, further demonstrating the effectiveness of CMM in mitigating the modality gap.

5 Ablation Study

In this section, we conduct several ablation experiments on both CMM and $\text{Logits}_{\text{CMM}}$ using the RN50 to investigate the role of integrating CLIP's inter-modal classification and the impact of the modality gap in pretrained vision-language models on the representation of class prototypes.

Ablations of CMM We evaluated three key components of CMM. As shown in Table 5, the basic $\text{Logits}_{\text{CMM}}$ configuration achieved an initial classification accuracy. Incorporating the triplet loss function led to a 0.37% increase in accuracy, indicating that $\text{L}_{\text{triplet}}$ effectively enhances the local alignment between text and image features. Combining $\text{Logits}_{\text{CMM}}$ with $\text{Logits}_{\text{CLIP}}$ further improved the accuracy by 0.86%, demonstrating the effective utilization of pretrained vision-language knowledge. Finally, adjusting the fusion coefficient α and integrating it with $\text{Logits}_{\text{CLIP}}$ resulted in a 1.92% accuracy gain, validating the role of α in adapting to downstream tasks.

$\text{Logit}_{\text{CMM}}$	$\text{Logit}_{\text{CLIP}}$	α	$\text{L}_{\text{triplet}}$	Top1(%)
✓	×	×	×	64.02
✓	×	×	✓	64.39
✓	✓	×	×	64.88
✓	✓	×	✓	65.21
✓	✓	✓	×	65.94
✓	✓	✓	✓	66.17

Table 5: Results of an ablation study conducted on ImageNet using RN50, summarizing the impact of various components on the performance of the integrated CLIP inter-modal classifier.

Method	W	$\text{Logit}_{\text{triplet}}$	ImageNet	Flowers	EuroSAT
$\text{Logit}_{\text{CMM}}$	×	×	61.13	95.94	85.37
$\text{Logit}_{\text{CMM}}$	×	✓	61.20	96.14	85.72
$\text{Logit}_{\text{CMM}}$	✓	×	64.02	96.91	86.20
$\text{Logit}_{\text{CMM}}$	✓	✓	64.39	97.24	86.69

Table 6: Results of an ablation study conducted on ImageNet, Flowers, and EuroSAT using RN50, summarizing the impact of the modality gap on class prototype representation.

Ablations of Logits$_{\text{CMM}}$ In Table. 6, we conduct an ablation study on the Logits$_{\text{CMM}}$ component to assess how the linear transformation matrix W and the triplet loss affect class prototype representation. The modality gap, which causes misalignment between image and text features, hinders the accurate representation of class prototypes. Without addressing this gap, the performance is limited. Applying the linear transformation W maps image features to the text feature space, achieving global alignment, while the triplet loss refines local relationships, enhancing the integration of text features into image feature clusters. Combining both effectively mitigates the modality gap, enabling text features to serve as accurate class prototypes, as shown in Fig. 8.

6 Conclusion

In this study, we systematically analyze the modality gap in pre-trained vision-language models (VLMs), revealing its adverse effects on class prototype representation and few-shot image classification performance. To address this, we propose a Cross-Modal Mapping (CMM) method that aligns image and text features using linear transformation and triplet loss, thereby improving classification performance, as supported by our experiments. Experimental results show that CMM improves the average Top-1 accuracy by 1.06% on 11 benchmark datasets compared to backbone fine-tuning methods and exhibits good generalization on 4 distribution-shifted datasets. The CMM method is designed to be simple and efficient, making it highly suitable for data-scarce scenarios. In the future, we plan to explore dynamic alignment strategies to further enhance the method's robustness in fine-grained classification and adversarial environments.

References

Lukas Bossard, Matthieu Guillaumin, and Luc Van Gool. Food-101–mining discriminative components with random forests. In *Computer vision–ECCV 2014: 13th European conference, zurich, Switzerland, September 6-12, 2014, proceedings, part VI 13*, pp. 446–461. Springer, 2014.

Bolun Cai, Pengfei Xiong, and Shangxuan Tian. Center contrastive loss for metric learning. *arXiv preprint arXiv:2308.00458*, 2023.

Jia Chen, Yinfei Yang, Ye Xia, Yi-Ting Chen, Zarana Parekh, Hieu Pham, QuocV. Le, Yun-Hsuan Sung, Zhen Li, and Tom Duerig. Scaling up visual and vision-language representation learning with noisy text supervision. *Cornell University - arXiv,Cornell University - arXiv*, Feb 2021.

Mircea Cimpoi, Subhransu Maji, Iasonas Kokkinos, Sammy Mohamed, and Andrea Vedaldi. Describing textures in the wild. In *Proceedings of the IEEE conference on computer vision and pattern recognition*, pp. 3606–3613, 2014.

Jia Deng, Wei Dong, Richard Socher, Li-Jia Li, Kai Li, and Li Fei-Fei. Imagenet: A large-scale hierarchical image database. In *2009 IEEE conference on computer vision and pattern recognition*, pp. 248–255. Ieee, 2009.

Alexey Dosovitskiy. An image is worth 16x16 words: Transformers for image recognition at scale. *arXiv preprint arXiv:2010.11929*, 2020.

Aleksandr Ermolov, Leyla Mirvakhabova, Valentin Khrulkov, Nicu Sebe, and Ivan Oseledets. Hyperbolic vision transformers: Combining improvements in metric learning. In *Proceedings of the IEEE/CVF Conference on Computer Vision and Pattern Recognition*, pp. 7409–7419, 2022.

Li Fei-Fei, Rob Fergus, and Pietro Perona. Learning generative visual models from few training examples: An incremental bayesian approach tested on 101 object categories. In *2004 conference on computer vision and pattern recognition workshop*, pp. 178–178. IEEE, 2004.

Chelsea Finn, Pieter Abbeel, and Sergey Levine. Model-agnostic meta-learning for fast adaptation of deep networks. In *International conference on machine learning*, pp. 1126–1135. PMLR, 2017.

Peng Gao, Shijie Geng, Renrui Zhang, Teli Ma, Rongyao Fang, Yongfeng Zhang, Hongsheng Li, and Yu Qiao. Clip-adapter: Better vision-language models with feature adapters. *International Journal of Computer Vision*, 132(2):581–595, 2024.

Xiuye Gu, Tsung-Yi Lin, WenChuan Kuo, and Yin Cui. Open-vocabulary object detection via vision and language knowledge distillation. *Learning,Learning*, Apr 2021.

Kaiming He, Xiangyu Zhang, Shaoqing Ren, and Jian Sun. Delving deep into rectifiers: Surpassing human-level performance on imagenet classification. In *2015 IEEE International Conference on Computer Vision (ICCV)*, Dec 2015. doi: 10.1109/iccv.2015.123. URL `http://dx.doi.org/10.1109/iccv.2015.123`.

Kaiming He, Xiangyu Zhang, Shaoqing Ren, and Jian Sun. Deep residual learning for image recognition. In *Proceedings of the IEEE conference on computer vision and pattern recognition*, pp. 770–778, 2016.

Patrick Helber, Benjamin Bischke, Andreas Dengel, and Damian Borth. Eurosat: A novel dataset and deep learning benchmark for land use and land cover classification. *IEEE Journal of Selected Topics in Applied Earth Observations and Remote Sensing*, 12(7):2217–2226, 2019.

Dan Hendrycks, Steven Basart, Norman Mu, Saurav Kadavath, Frank Wang, Evan Dorundo, Rahul Desai, Tyler Zhu, Samyak Parajuli, Mike Guo, et al. The many faces of robustness: A critical analysis of out-of-distribution generalization. In *Proceedings of the IEEE/CVF international conference on computer vision*, pp. 8340–8349, 2021a.

Dan Hendrycks, Kevin Zhao, Steven Basart, Jacob Steinhardt, and Dawn Song. Natural adversarial examples. In *Proceedings of the IEEE/CVF conference on computer vision and pattern recognition*, pp. 15262–15271, 2021b.

DiederikP. Kingma and Max Welling. Vae. *arXiv: Machine Learning,arXiv: Machine Learning*, Dec 2013.

Jonathan Krause, Michael Stark, Jia Deng, and Li Fei-Fei. 3d object representations for fine-grained categorization. In *Proceedings of the IEEE international conference on computer vision workshops*, pp. 554–561, 2013.

Zhenguo Li, Fengwei Zhou, Fei Chen, and Hang Li. Meta-sgd: Learning to learn quickly for few-shot learning. *arXiv preprint arXiv:1707.09835*, 2017.

Victor Weixin Liang, Yuhui Zhang, Yongchan Kwon, Serena Yeung, and James Y Zou. Mind the gap: Understanding the modality gap in multi-modal contrastive representation learning. *Advances in Neural Information Processing Systems*, 35:17612–17625, 2022.

Zhiqiu Lin, Samuel Yu, Zhiyi Kuang, Deepak Pathak, and Deva Ramanan. Multimodality helps unimodality: Cross-modal few-shot learning with multimodal models. In *Proceedings of the IEEE/CVF Conference on Computer Vision and Pattern Recognition*, pp. 19325–19337, 2023.

I Loshchilov. Decoupled weight decay regularization. *arXiv preprint arXiv:1711.05101*, 2017.

Ilya Loshchilov and Frank Hutter. Sgdr: Stochastic gradient descent with warm restarts. *arXiv: Learning,arXiv: Learning*, Aug 2016.

Laurensvander Maaten and GeoffreyE. Hinton. Visualizing data using t-sne. *Journal of Machine Learning Research,Journal of Machine Learning Research*, Jan 2008.

Subhransu Maji, Esa Rahtu, Juho Kannala, Matthew Blaschko, and Andrea Vedaldi. Fine-grained visual classification of aircraft. *arXiv preprint arXiv:1306.5151*, 2013.

Fausto Milletari, Nassir Navab, and Seyed-Ahmad Ahmadi. V-net: Fully convolutional neural networks for volumetric medical image segmentation. In *2016 fourth international conference on 3D vision (3DV)*, pp. 565–571. Ieee, 2016.

Maria-Elena Nilsback and Andrew Zisserman. Automated flower classification over a large number of classes. In *2008 Sixth Indian conference on computer vision, graphics & image processing*, pp. 722–729. IEEE, 2008.

Rasmus Palm, Ulrich Paquet, and Ole Winther. Recurrent relational networks. *Advances in neural information processing systems*, 31, 2018.

Omkar M Parkhi, Andrea Vedaldi, Andrew Zisserman, and CV Jawahar. Cats and dogs. In *2012 IEEE conference on computer vision and pattern recognition*, pp. 3498–3505. IEEE, 2012.

Fang Peng, Xiaoshan Yang, and Changsheng Xu. Sgva-clip: Semantic-guided visual adapting of vision-language models for few-shot image classification. Nov 2022.

Alec Radford, Jong Wook Kim, Chris Hallacy, Aditya Ramesh, Gabriel Goh, Sandhini Agarwal, Girish Sastry, Amanda Askell, Pamela Mishkin, Jack Clark, et al. Learning transferable visual models from natural language supervision. In *International conference on machine learning*, pp. 8748–8763. PMLR, 2021.

Benjamin Recht, Rebecca Roelofs, Ludwig Schmidt, and Vaishaal Shankar. Do imagenet classifiers generalize to imagenet? In *International conference on machine learning*, pp. 5389–5400. PMLR, 2019.

Jake Snell, Kevin Swersky, and Richard Zemel. Prototypical networks for few-shot learning. *Advances in neural information processing systems*, 30, 2017.

Khurram Soomro, Amir Roshan Zamir, and Mubarak Shah. A dataset of 101 human action classes from videos in the wild. *Center for Research in Computer Vision*, 2(11):1–7, 2012.

Yi-Lin Sung, Jaemin Cho, and Mohit Bansal. Vl-adapter: Parameter-efficient transfer learning for vision-and-language tasks. In *Proceedings of the IEEE/CVF conference on computer vision and pattern recognition*, pp. 5227–5237, 2022.

Yuwei Tang, Zhenyi Lin, Qilong Wang, Pengfei Zhu, and Qinghua Hu. Amu-tuning: Effective logit bias for clip-based few-shot learning.

Oriol Vinyals, Charles Blundell, Timothy Lillicrap, Daan Wierstra, et al. Matching networks for one shot learning. *Advances in neural information processing systems*, 29, 2016.

Haohan Wang, Songwei Ge, Zachary Lipton, and Eric P Xing. Learning robust global representations by penalizing local predictive power. *Advances in Neural Information Processing Systems*, 32, 2019.

Xin Wang, Thomas E Huang, Trevor Darrell, Joseph E Gonzalez, and Fisher Yu. Frustratingly simple few-shot object detection. *arXiv preprint arXiv:2003.06957*, 2020.

Mitchell Wortsman, Gabriel Ilharco, Jong Wook Kim, Mike Li, Simon Kornblith, Rebecca Roelofs, Raphael Gontijo Lopes, Hannaneh Hajishirzi, Ali Farhadi, Hongseok Namkoong, et al. Robust fine-tuning of zero-shot models. In *Proceedings of the IEEE/CVF conference on computer vision and pattern recognition*, pp. 7959–7971, 2022.

Jianxiong Xiao, James Hays, Krista A Ehinger, Aude Oliva, and Antonio Torralba. Sun database: Large-scale scene recognition from abbey to zoo. In *2010 IEEE computer society conference on computer vision and pattern recognition*, pp. 3485–3492. IEEE, 2010.

Ruihan Yang, Huazhe Xu, Yi Wu, and Xiaolong Wang. Multi-task reinforcement learning with soft modularization. *Advances in Neural Information Processing Systems*, 33:4767–4777, 2020.

Tianhe Yu, Deirdre Quillen, Zhanpeng He, Ryan Julian, Karol Hausman, Chelsea Finn, and Sergey Levine. Meta-world: A benchmark and evaluation for multi-task and meta reinforcement learning. In *Conference on robot learning*, pp. 1094–1100. PMLR, 2020.

Lu Yuan, Dongdong Chen, Yi-Ling Chen, Noel Codella, Xiyang Dai, Jianfeng Gao, Houdong Hu, Xuedong Huang, Boxin Li, Chunyuan Li, Ce Liu, Mengchen Liu, Zicheng Liu, Yumao Lu, Yu Shi, Lijuan Wang, Jianfeng Wang, Bin Xiao, Zhen Xiao, Jianwei Yang, Michael Zeng, Luowei Zhou, and Pengchuan Zhang. Florence: A new foundation model for computer vision.

Renrui Zhang, Rongyao Fang, Wei Zhang, Peng Gao, Kunchang Li, Jifeng Dai, Yu Qiao, and Hongsheng Li. Tip-adapter: Training-free clip-adapter for better vision-language modeling. *arXiv preprint arXiv:2111.03930*, 2021.

Xiaochen Zheng. Rare wildlife recognition with self-supervised representation learning. *arXiv preprint arXiv:2211.05636*, 2022.

Kaiyang Zhou, Jingkang Yang, Chen Change Loy, and Ziwei Liu. Conditional prompt learning for vision-language models. In *Proceedings of the IEEE/CVF conference on computer vision and pattern recognition*, pp. 16816–16825, 2022.

Beier Zhu, Yulei Niu, Yucheng Han, Yue Wu, and Hanwang Zhang. Prompt-aligned gradient for prompt tuning. In *Proceedings of the IEEE/CVF International Conference on Computer Vision*, pp. 15659–15669, 2023.

7 Appendix

7.1 Nonlinear mapping analysis.

To investigate the impact of nonlinear transformations on our Cross-Modal Mapping (CMM) method, we introduce ReLU activation functions between layers to construct nonlinear mappings of varying depths. Specifically, we design a multi-layer mapping architecture where each layer consists of a linear transformation (with dimensionality $d = 1024$, matching CLIP's embedding size) followed by residual connections and ReLU activations. The results of this ablation study on ImageNet under the 16-shot setting are presented in Table. 7.

Notably, as the number of nonlinear layers increases from zero (linear mapping) to five, the model's top-1 accuracy declines progressively from 66.17% to 65.14%. This trend suggests that, unlike traditional deep learning tasks where nonlinearity often enhances expressiveness, nonlinear mappings are detrimental in our few-shot cross-modal context.

We hypothesize that this performance degradation arises from several fundamental issues inherent to few-shot learning and cross-modal tasks. Below, we explore these factors in depth to explain why nonlinear mappings underperform in such scenarios.

Table 7: Nonlinear mapping ablation on ImageNet under the 16-shot.

linear	2 nonlinear	3 nonlinear	4 nonlinear	5 nonlinear
66.17	65.88	65.83	65.57	65.14

Increased Risk of Overfitting. In few-shot learning, training samples are severely limited (e.g., 16-shot or even 1-shot). Nonlinear mappings significantly increase model complexity by introducing additional parameters—from d^2 in a single linear layer to $k \cdot d^2$ for k nonlinear layers. This expanded capacity heightens the risk of overfitting, as the model tends to memorize noise or idiosyncrasies in the sparse training data rather than learning generalizable patterns. Consequently, while a linear mapping maintains simplicity and robustness, nonlinear mappings exacerbate overfitting, leading to poorer test-set performance.

Disruption of Pre-trained Cross-Modal Alignment. CLIP aligns image and text features in a joint embedding space through contrastive learning, relying on linear transformations to preserve geometric relationships. Nonlinear transformations, such as ReLU, introduce distortions that warp this pre-trained alignment. This misalignment hinders the ability of triplet loss to optimize cross-modal similarities, as the distorted feature space disrupts the optimization process of text features.

Feature Distribution Mismatch. To quantify the impact of nonlinearity on feature distributions, we compute the Kullback-Leibler (KL) divergence between mapped image features and text features. With linear mapping, the KL divergence is low (0.075, as shown in Fig. 6), indicating strong distributional similarity. However, with five nonlinear layers, it rises sharply (3.13), confirming that nonlinearity excessively distorts the feature space. This mismatch disrupts the accuracy of class prototypes, directly impairing classification performance in cross-modal tasks.

Supporting Evidence and Contextual Insights. These findings align with prior research in few-shot learning, where simpler models often outperform complex ones due to their reduced propensity for overfitting Snell et al. (2017). In cross-modal settings, maintaining pre-trained alignment is paramount, and excessive transformations can destabilize this balance Liang et al. (2022). To further validate our analysis, we evaluated nonlinear mappings in more challenging scenarios: the single-sample setting and the fine-grained dataset (FGVC Aircrafts). As shown in Table. 8, the performance drop is more significant (with the 5 nonlinear mapping being 3.38% lower than the linear mapping), highlighting the limitations of nonlinear mappings in situations of extreme data scarcity or high inter-class similarity.

7.2 Grid search for the best α value.

During the inference phase, we conducted a grid search for α on the validation set, with the search range set from 0.1 to 1.0 and a step size of 0.1. As shown in Table 9, through this process

Table 8: Nonlinear mapping ablation on FGVC Aircrafts under the 1-shot.

linear	2 nonlinear	3 nonlinear	4 nonlinear	5 nonlinear
21.84	20.38	19.73	19.12	18.46

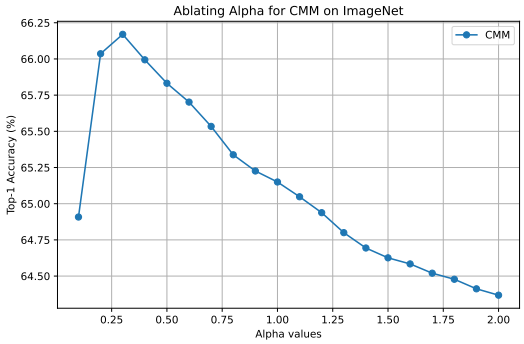

Figure 9: α search results on ImageNet.

we determined the optimal α value for each dataset. The discovery of these optimal α values is significant because they can effectively integrate the inter-modal contributions from the original CLIP and the cross-modal contributions from $\text{Logits}_{\text{CMM}}$, and also indicate that due to the reduction of the modality gap, the search space for α has become smaller. Compared to other methods that require extensive hyperparameter tuning, this significantly reduces the search time and computational resource requirements. Additionally, as shown in Figure 9, we also report the results of expanding the search range to [0.1, 2.0] with a step size of 0.1 on the ImageNet dataset.

Table 9: Best α for 16-shot test on various datasets

Dataset	α
Caltech101	0.7
DTD	0.6
EuroSAT	0.8
FGVC Aircrafts	0.6
Food101	0.2
ImageNet	0.3
Oxford Flowers	0.6
Oxford Pets	0.2
Stanford Cars	0.6
SUN397	0.5
UCF101	0.3

7.3 Detailed results for each dataset.

In Fig. 14, we present the detailed performance of CMM across various datasets and compare it with both the inter-modal classification method (Cross-Modal Linear (Lin et al., 2023)) and the intra-modal classification method (TIP-Adapter-F (Zhang et al., 2021)). Notably, CMM significantly outperforms the Cross-Modal Partial method (Lin et al., 2023), which involves partial fine-tuning of the encoder. This result strongly validates and reinforces our argument.

7.4 Complexity analysis.

The CMM method exhibits low computational complexity. Its core step involves mapping image features to the text space using a linear transformation matrix $W \in \mathbb{R}^{d\times d}$, with a computational cost

Figure 10: Minimal textual description differences for aircraft like Boeing 767 and Boeing 777 in the FGVC Aircrafts.

of $O(B \times d^2)$. The computation of the loss functions (cross-entropy and triplet loss) is $O(B \times d \times N)$, where N denotes the number of categories. Thus, the overall complexity is $O(B \times d \times N + B \times d^2)$.

7.5 Error Case Analysis.

Error cases can generally be categorized into four scenarios: 1) poor performance on specific categories. 2) degraded performance with extremely few samples (1-shot). 3) errors when encountering adversarial images, and 4) performance decline under distribution shifts. Below, we provide a detailed analysis of each scenario:

1) As shown in Fig. 14 (c), in the 16-shot scenario on the FGVC Aircrafts dataset, CMM's accuracy is slightly lower than that of methods employing partial fine-tuning. This is because CMM relies on textual descriptions as class prototypes. However, in this dataset, the textual descriptions of different aircraft models are very similar (as shown in Fig. 10, Boeing 767 and Boeing 777 exhibit minimal semantic differences). Therefore, the text features fail to provide sufficient discriminability.

2) As shown in Fig. 14, due to insufficient sample size, the 1-shot accuracy of CMM fluctuates significantly across 11 datasets. This instability stems from the insufficient number of samples, which hinders effective modality alignment. In the 1-shot scenario, the linear transformation struggles to learn a generalized mapping from a single image sample to the text feature space, leading to misalignment. Additionally, the triplet loss, which relies on multiple samples, cannot adequately optimize feature relationships with only one positive sample, resulting in unstable decision boundaries. Furthermore, the quality of the single sample significantly impacts performance. If it does not represent its class well, the alignment suffers.

3) Taking ImageNet-A (an adversarial sample dataset) as an example, the results in Table. 3 indicate that all compared methods experience a significant drop in accuracy. Nevertheless, CMM maintains competitive performance. This suggests that while CMM is not entirely immune to adversarial interference, it exhibits relatively strong robustness compared to other methods.

4) In Table. 3, an OOD (Out-of-Distribution) evaluation was conducted, and the results show that CMM consistently delivers competitive performance when faced with distribution shifts. This underscores CMM's advantage in generalization, as it sustains robust performance even when the data distribution changes.

7.6 Benefits of Mitigating the Modality Gap.

As shown in Fig. 11, we compare the cosine similarity between CLIP's inter-modal classifier and our $\text{Logits}_{\text{CMM}}$ cross-modal classifier using 4,000 images from ImageNet not seen during training. The results demonstrate that $\text{Logits}_{\text{CMM}}$ outperforms CLIP's inter-modal representations in three key aspects: 1) Higher cosine similarity for matching modalities, indicating better alignment and fusion of cross-modal features; 2) Lower cosine similarity for non-matching modalities, showing improved

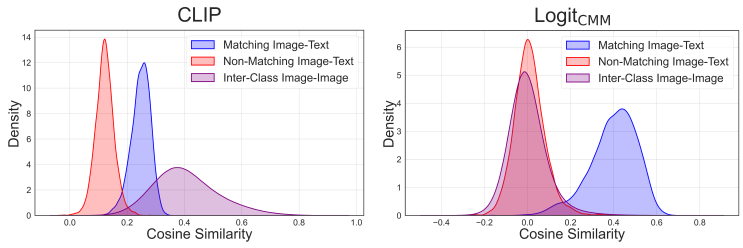

Figure 11: Comparison of Inter-Modal and Inter-Class Similarity between CLIP and CMM: We evaluate using cosine similarity. CMM minimizes inter-class similarity within the image modality and inter-modal mismatched similarity, while maximizing inter-modal matched similarity, thereby better mitigating the modality gap.

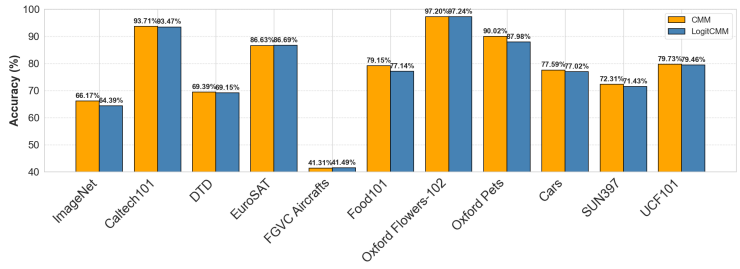

Figure 12: Comparison of the Top-1 accuracy between CMM and Logits$_{CMM}$ on 11 datasets under the 16-shot.

ability to distinguish between different modalities and reduce mismatches; 3) Lower inter-class cosine similarity within the image modality, reflecting clearer category distinctions. Additionally, as shown in Fig. 12, Logits$_{CMM}$ achieves performance comparable to or better than CMM across 11 datasets, with improvements on EuroSAT (+0.06%) and FGVC Aircrafts (+0.18%). This indicates that mitigating the modality gap not only enhances cross-modal consistency but also improves the model's generalization ability across different datasets.

7.7 The integration is a reasonable strategy.

Intuitively, the inter-modal classification of the pre-trained CLIP generates errors that are highly unrelated to the correct outputs. This means that we can achieve error reversal by integrating with it. As shown in Fig. 13, we display the proportion of inconsistency errors and the proportion of

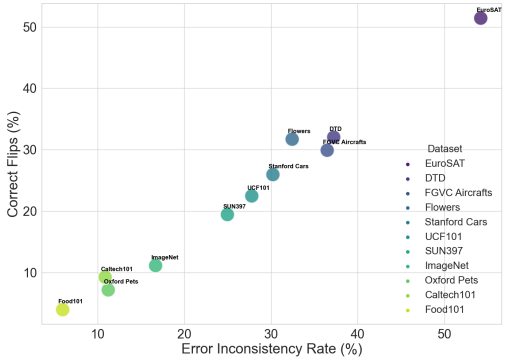

Figure 13: Comparison of correct flips rate and error inconsistency rate between CMM and CLIP in 16-shot learning across 11 datasets.

correct reversals of CMM across 11 datasets. Specifically, datasets with a higher proportion of inconsistency errors often have a higher rate of correct reversals, indicating that although errors occur frequently, their patterns are relatively consistent, making it possible to correct errors through integration methods. Moreover, reversing the errors produced by the pretrained CLIP does not render it meaningless. As shown in Fig. 12, CMM outperforms $\text{Logits}_{\text{CMM}}$ by 2.15% on ImageNet, indicating that CMM can still leverage the pretraining knowledge provided by CLIP's inter-modal classification.

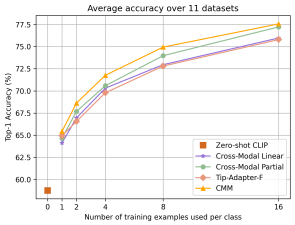

(a) Average Accuracy over 11 datasets

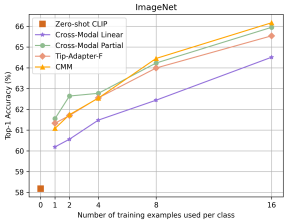

(b) ImageNet

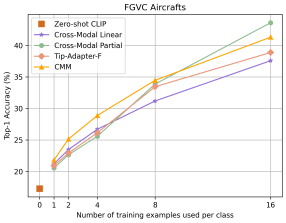

(c) FGVC Aircrafts

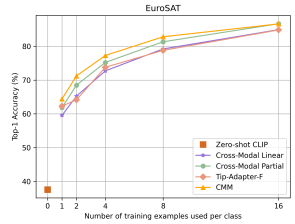

(d) EuroSAT

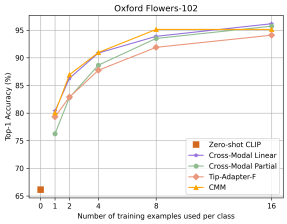

(e) Oxford Flowers-102

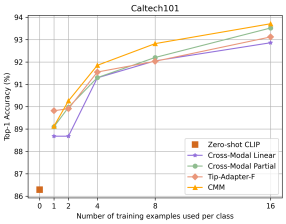

(f) Caltech101

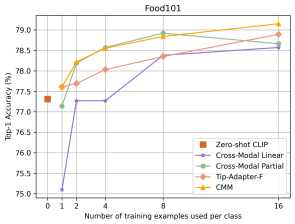

(g) Food101

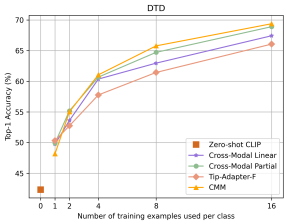

(h) DTD

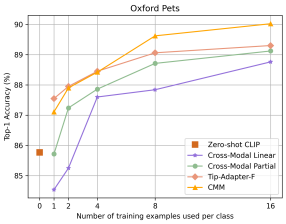

(i) Oxford Pets

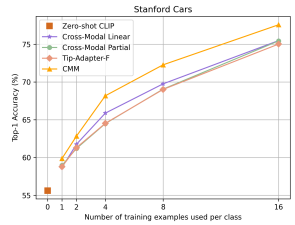

(j) Stanford Cars

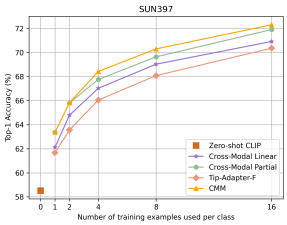

(k) SUN397

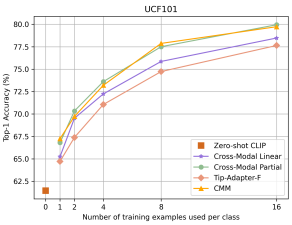

(l) UCF101

Figure 14: Comparison of few-shot image classification results across 11 datasets. Compared to previous inter-modal and intra-modal classifiers, our Cross-Modal Mapping (CMM) method effectively mitigates the modality gap in pretrained vision-language models and consistently demonstrates significant advantages across all datasets.